NASA Technical Memorandum 100966

Optical Measurement of Unducted Fan Blade Deflections

Anatole P. Kurkov
Lewis Research Center
Cleveland, Ohio

Prepared for the
34th International Gas Turbine and Aeroengine Congress and Exposition
sponsored by the American Society of Mechanical Engineers
Toronto, Canada, June 4–8, 1989

NASA

OPTICAL MEASUREMENT OF UNDUCTED FAN BLADE DEFLECTIONS

Anatole P. Kurkov
National Aeronautics and Space Administration
Lewis Research Center
Cleveland, Ohio 44135

ABSTRACT

A nonintrusive optical method for measuring unducted fan (or propeller) blade deflections is described and evaluated. The measurement does not depend on blade surface reflectivity. Deflection of a point at the leading edge and a point at the trailing edge in a plane nearly perpendicular to the pitch axis is obtained with a single light beam generated by a low-power, helium-neon laser. Quantitative analyses are performed from taped signals on a digital computer. Averaging techniques are employed to reduce random errors. Measured static deflections from a series of high-speed wind tunnel tests of a counterrotating unducted fan model are compared with available predicted deflections, which are also used to evaluate systematic errors.

INTRODUCTION

In this method a concentrated light beam, such as generated by a laser, is directed to the blade pressure surface in a plane approximately perpendicular to the pitch axis. The incident light beam forms a small angle relative to the chord, usually about 10°. The overall schematic of the experiment is given in Fig. 1, and the relationship of the beam and the undeflected and deflected blades in Fig. 2. (Note that in this figure the coordinate system is fixed with respect to the blade.) As the blades rotate, the leading and trailing edges intersect the light beam. Therefore by placing a photodetector in the light beam path on the opposite test section wall, one can obtain a series of negative pulses, each associated with the period of time when the light was shadowed from the detector by a blade. If in addition a once-per-revolution reference pulse is generated, these pulses can provide an indication of the instantaneous blade positions for each revolution in a rotating reference frame. This method complements the already established optical blade deflection method (Nieberding and Pollack, 1977; Kurkov, 1984; Lawrence and Meyn, 1985), which relies on blade tip reflection of the incident light beam and thus requires that the casing be close to the blade tips.

Other available methods for measuring blade deflections that, like the present method, do not require the close proximity of the rotor casing are either intrusive or rely on photographic records or visual observation (Taylor, 1935; Stargardter, 1977; Srinivasan and Fulton, 1984). All quantitative analyses in the present method are performed from the taped signals on a minicomputer. Random errors are reduced by averaging in the time and space domains. Note also that, unlike in the reflected-light method, here one light beam essentially measures the deflection of two points, one at the leading and one at the trailing edge, and the measurement does not depend on surface reflectivity.

Experimental data from the high-speed test of a series of 0.61-m-diameter model rotors incorporated in a counterrotating, unducted fan arrangement built by the General Electric Company illustrate the use of the method. The test was performed in the NASA Lewis Research Center's 8- by 6-ft (2.44- by 1.83-m) wind tunnel (Fig. 3). In this figure the laser beam is shown intercepted by a blade tip. All the blades tested had a composite shell. Their plan view is given in Fig. 4. Additional information on the F7 blade and its performance is available (Sullivan, 1987).

This report also includes predicted deflections that were obtained from the aerostructural, finite-element code outputs supplied by the manufacturer. To compare experimental and predicted deflections, one can always calculate the particular deflection component that is being measured. However, because in the present case the measured component is not a generally accepted or easily defined quantity, and because it could easily be misinterpreted, the more commonly accepted deflection parameters such as bending and twist deflections were derived from experimental measurements and compared with predictions. Both these deflections can be obtained from measurements because they depend on the displacement perpendicular to the chord and the light beam makes only a small angle relative to the chord. The errors associated with these estimates are largely caused by the finite incidence angle of the laser beam relative to the blade and the fact that the sensor (i.e., the combination of laser

beam and detector) is fixed in space, and not with respect to the blade as is a strain gage, for example. The net effect is that a blade edge is free to slip relative to the laser beam during blade deformation. Because these errors are inherent in the experimental procedure, they can be classified as systematic, or bias, errors.

The measured twist and bending deflections can only be relied upon if one shows that these errors are small. Systematic errors are estimated by cutting the finite-element, deflected-blade contour with a line coincident with the laser beam in the same way that the real deflected blade is cut by a laser beam during the test. Since in this case the true displacements of the original contact points between the undeflected blade and the laser beam are also known, the incidence and the slip effects can be evaluated.

Note that when exact knowledge of the deflected-blade shape is assumed in this paper, it is to illustrate where the measured deflections fall short of the true deflections and to estimate systematic errors. Only the undeflected-blade, finite-element contour is used for defining the initial geometric conditions for measured deflections.

Because only incomplete information was available for the F21 blade, the systematic-error analysis for this blade could not be fully completed. For this reason, the F21 results are presented separately in the last part of the section "Results."

EXPERIMENTAL MEASUREMENTS

Experimental Equipment

Low-power, helium-neon lasers were selected for this experiment because of their low cost and rugged, compact construction and because they provide a monochromatic light source. Large-area silicon photodiodes manufactured by United Detector Technology (UDT) were selected for the detectors. The detector output was coupled to UDT model 201A amplifier. The data were recorded on the frequency-modulated wideband II tape recorder at 120 in./sec (304.8 cm/sec).

This basic system, consisting of a laser and a photodiode, was enhanced by using a commercial beam expander to focus the laser beam onto a blade, and by using an optical line filter to shield the extraneous light from the detector. The overall experiment schematic is given in Fig. 1.

In addition to the blade signals it was also necessary to generate a once-per-revolution signal of the same quality. This was achieved by attaching a small mirror to the fan hub and reflecting the nearly perpendicular incident laser beam onto a photodiode detector placed (at the time of reflection) opposite the mirror. For assurance that optical alignment was not changed during a run, alignment checks were made before and after each test run.

Laser Beam Alignment

Figure 2 describes the geometry of the laser beam and the deflected and undeflected blades, neglecting the deviations away from the XY plane. The coordinate system is fixed with respect to the blade. The Y axis is coincident with the rotational axis, and the Z axis is coincident with the blade pitch axis and points upward. Lines that are either in the direction of the average chord line or are perpendicular to it are shown as dashed lines for ease of recognition.

The laser beam entered the tunnel through one of the boundary layer bleed holes (Fig. 3). The hole was selected so that the following requirements were met as closely as possible: (1) the trace of the beam on the blade pressure surface was coincident with a marked line perpendicular to the pitch axis; (2) the incidence on the blade was less than 12° but sufficiently high so that the beam was either cut or uncovered only by the blade edges and required only a small rotation to complete the intersection; and (3) the beam tilt relative to the axis was sufficient to pass the beam past one of the blade rows and at the same time have it incident on the upstream window area.

In this report only the data for the forward rotor are presented. For it, the tilt direction required to bypass the rear rotor was toward the axis, the same direction required by the tunnel window.

The laser beam intercepts at the leading and trailing edges on the alignment blade could be easily located by rotating this blade slightly and observing the beam trace on the blade. The tangential length of the trace (distance AA in Fig. 2) and the incidence angle γ between it and the beam were also measured directly. This, together with the known finite-element description of the undeflected blade, was sufficient to define measured twist and bending parameters.

Experimental Data Reduction

Prerecorded signals from the magnetic tape were processed on a system consisting of a minicomputer, an eight-channel digitizer, and high-volume disk storage peripherals. It was determined that about 12 000 points per revolution provided sufficient resolution for the recorded signals. An example of each pulse after it was digitized is given in Figs. 5 and 6.

The once-per-revolution pulse subdivides the continuous blade-pulse train into consecutive revolutions. From this one can obtain the shaft rotational speed and then express each blade pulse position in terms of a relative angular coordinate in the rotational plane. These blade positions were typically averaged over about 50 revolutions.

The data were taken at some low reference speed, where blade deflections were very small and consequently could be neglected, and at higher speeds including the design speed, where deflections were significant. Subtracting the two corresponding angular positions in the rotational plane for a particular blade gives angular deflection in the tangential direction (i.e., the polar angle subtended by vector $\mathbf{d}_t$ in Fig. 2). The tangential deflections were then spatially averaged over all blades. Depending on the model the number of blades varied from 8 to 11. Note that for static deflections spatial averaging is necessary to eliminate a possible dynamic component resulting from the engine-order excitations. These signals cannot be eliminated by time averaging, which only removes the self-excited dynamic signals such as flutter.

ANALYSIS

In Fig. 2 the deflected and undeflected chords are purposely shown to be different in length. To a large extent this is caused by the fact that the blade is free to slip relative to the laser beam as dictated by the geometry of the deflected blade and the beam. Because of the unequal sweeps at blade leading and trailing edges, any slip along the radial direction will be reflected in Fig. 2 as a change in the apparent deflected-blade chord length. Since experimental twist angle is essentially computed from the change in the projected chord length in the tangential direction, the apparent chord-length change caused by the slip effect will introduce an error in the measured twist. So that this error can be evaluated, experimental conditions are simulated by cutting the calculated deflected-blade contour with a line coincident with the laser beam

rotating in the relative reference frame. Since the entire calculated deflected-blade section is known, one can evaluate the twist angle with and without assuming constant chord length. Note, however, that even when the chord-length change in predicted results has been accounted for, there remains some slip effect because points A and A' for undeflected and predicted deflected sections are not necessarily associated with the same blade particles. Hence one should also obtain the predicted twist angle strictly by following the blade particles at the leading and trailing edges, where the beam is tangent to the undeflected blade. Although both errors are largely caused by the fact that the blade is free to slip relative to the beam, to differentiate between these errors, the first will be referred to as the error due to the constant-chord assumption, and the second will simply be referred to as the slip effect error.

Linear interpolation is used to evaluate the coordinates of point A' from the predicted deflected-blade contour for the case of true deflection (i.e., following the blade particle associated with point A). Coordinates of points A at the leading and trailing edges are known from initial conditions, and the coordinates of the end points of finite-element edge segments for undeflected- and deflected-blade contours are available from the finite-element code outputs. (The appropriate edge segments are selected so that in the undeflected configuration they contain points A.) To evaluate coordinates of points A' for simulated experimental conditions, one must obtain equations of lines containing appropriate edge segments as well as the equation of the line coincident with the laser beam as depicted in Fig. 2. Rotating this line until it intersects either edge-segment line results in a quadratic equation whose solution gives coordinates of associated points A' (Kurkov, 1988).

There are three displacement vector diagrams in Fig. 2. In the first the total displacement $\mathbf{d}$ is resolved in the tangential direction and along the laser beam. Thus

$$\mathbf{d} = \mathbf{d}_t + \mathbf{d}_L \tag{1}$$

The second vector diagram, given by

$$\mathbf{d} = \mathbf{d}_c + \mathbf{h} \tag{2}$$

resolves vector $\mathbf{d}$ along the average chord direction and perpendicular to it. These two vector diagrams assume knowledge of deflected-blade coordinates A', and therefore they can only be obtained for predicted results. In the experiment bending h and twist θ must be deduced from the measured tangential displacement d_t and the knowledge of angles β and γ (Fig. 2). Estimates for h and θ are obtained by resolving $\mathbf{d}_t$ into components perpendicular to the average chord, $\mathbf{h}_t$, and along the laser beam, $\mathbf{d}_\ell$. Thus

$$\mathbf{d}_t = \mathbf{d}_\ell + \mathbf{h}_t \tag{3}$$

which is the third vector diagram in Fig. 2. Note that quantities $\mathbf{h}$ and $\mathbf{d}$ cannot be obtained from the experiment because $\mathbf{d}_L$ and $\mathbf{d}_c$ cannot be measured with one laser beam. Thus Eqs. (1) and (2) are used only for predicted results. For experimental results Eq. (3) gives $\mathbf{h}_t$, which serves as an approximation to $\mathbf{h}$. (In the experiment the measured quantity is the polar angle subtended by vector $\mathbf{d}_t$. Thus $\mathbf{d}_t$ can be considered known.)

First, the exact equations will be given, that is, the equations assuming knowledge of the coordinates of points A and A'. For true deflections A and A' correspond to the same blade particles, and for simulated experimental results they are determined from the geometry of the laser beam and the blade. Subsequently, it will be shown how these equations are modified to obtain experimental deflections. Vector $\mathbf{h}$ is given by

$$\mathbf{h} = \mathbf{d} - \hat{\mathbf{c}}_a(\mathbf{d} \cdot \hat{\mathbf{c}}_a) \tag{4}$$

and its plane by

$$\hat{\mathbf{n}}_{ch} = \hat{\mathbf{c}}_a \times \hat{\mathbf{h}} \tag{5}$$

The average unit chord vector $\hat{\mathbf{c}}_a$ is the normalized average of the undeflected $\mathbf{c}$ and the deflected $\mathbf{c}'$ chords, which are defined as the difference between the leading- and trailing-edge point vectors r_A or $r_{A'}$ (Fig. 2). (Note that the primes are associated with the deflected-blade section.)

The polar angular coordinate φ is chosen to be positive opposite to the rotational direction. The average R direction is then defined by

$$\varphi_a = \left[\left(\varphi_A + \varphi_{A'}\right)_{LE} + \left(\varphi_A + \varphi_{A'}\right)_{TE}\right] \tag{6}$$

and the average bending plane by

$$\hat{\mathbf{n}}_h = \frac{\hat{\boldsymbol{\delta}}_{ta} \times \hat{\mathbf{c}}_a}{\left|\hat{\boldsymbol{\delta}}_{ta} \times \hat{\mathbf{c}}_a\right|} \tag{7}$$

where

$$\hat{\boldsymbol{\delta}}_{ta} = (\cos\varphi_a,\ 0,\ \sin\varphi_a) \tag{8}$$

Projection of h onto this plane is given by

$$\mathbf{h}_p = \mathbf{h} - \hat{\mathbf{n}}_h(\mathbf{h} \cdot \hat{\mathbf{n}}_h) \tag{9}$$

For simulated experimental conditions h_t is computed from

$$\hat{\mathbf{n}}_{t\ell} = \frac{\hat{\mathbf{d}}_t \times \hat{\mathbf{V}}_\ell}{\left|\hat{\mathbf{d}}_t \times \hat{\mathbf{V}}_\ell\right|} \tag{10}$$

$$\hat{\mathbf{h}}_t = \frac{\hat{\mathbf{c}}_a \times \hat{\mathbf{n}}_{t\ell}}{\left|\hat{\mathbf{c}}_a \times \hat{\mathbf{n}}_{t\ell}\right|} \tag{11}$$

$$h_t = \frac{d_t}{\hat{\mathbf{d}}_t \cdot \hat{\mathbf{h}}_t + \left|\hat{\mathbf{d}}_t \cdot \hat{\mathbf{V}}_\ell\right|\left|\hat{\mathbf{h}} \times \hat{\mathbf{d}}_t\right| \Big/ \left|\hat{\mathbf{d}}_t \times \hat{\mathbf{V}}_\ell\right|} \tag{12}$$

where $\hat{\mathbf{V}}_\ell$ is the unit vector in the laser beam direction pointing as shown in Fig. 2 and vector $\mathbf{d}_t$ can be computed given that its end points must lie on the constant R. Note that to obtain $\hat{\mathbf{V}}_\ell$ at the trailing edge, one must rotate the original $\hat{\mathbf{V}}_\ell$ at the leading

edge about the Y axis by the angle subtended by δ (Fig. 2). The plane of $\mathbf{h}_t$ is defined by the unit normal vector $\hat{\mathbf{n}}_t$ given by

$$\hat{\mathbf{n}}_t = \frac{\hat{\mathbf{h}}_t \times \hat{\mathbf{d}}_t}{\left|\hat{\mathbf{h}}_t \times \hat{\mathbf{d}}_t\right|} \tag{13}$$

Projection of $\mathbf{h}_t$ onto the plane defined by $\hat{\mathbf{n}}_h$ is denoted by $\mathbf{h}_{tp}$, and it is computed similarly to $\mathbf{h}_p$, Eq. (9).

The absolute twist angle is given by

$$\left|\theta_{n_c}\right| = \tan^{-1}\left|\frac{\mathbf{C}' \times \mathbf{C}}{\mathbf{C}' \bullet \mathbf{C}}\right| \tag{14}$$

$$\hat{\mathbf{n}}_c = \left|\frac{\mathbf{C}' \times \mathbf{C}}{\mathbf{C}' \times \mathbf{C}}\right| \tag{15}$$

Twist angle was also computed by projecting $\mathbf{C}$ and $\mathbf{C}'$ onto three other planes. Given that

$$\mathbf{C}_n = \mathbf{C} - \hat{\mathbf{n}}(\mathbf{C} \bullet \hat{\mathbf{n}}) \tag{16}$$

(and similarly for $\mathbf{C}_n'$), θ_n is computed from

$$\theta_n = \tan^{-1}\left[\frac{(\mathbf{C}_n' \times \mathbf{C}_n) \bullet \hat{\mathbf{n}}}{\mathbf{C}_n' \times \mathbf{C}_n}\right] \tag{17}$$

where $n_{c\ell}$, n_h, or k should be substituted for n. The unit vector $\hat{\mathbf{n}}_{c\ell}$ is defined by

$$\hat{\mathbf{n}}_{c\ell} = \frac{\left|\mathbf{C} \times \hat{\mathbf{V}}_\ell\right|}{\left|\mathbf{C} \times \hat{\mathbf{V}}_\ell\right|} \tag{18}$$

and $\hat{\mathbf{k}}$ denotes the unit vector for the Z axis.

Experimental Deflections

It is desirable to use the same set of equations for computing the predicted and experimental twist angles. However, in the experiment the coordinates of points A' and the deflected chord vector are unknown and must be obtained from some preliminary estimates of deflections in order to start the iteration. As an initial estimate of the twist angle the equation

$$C \sin\left(\frac{\theta}{2}\right) = \left(R_A\right)_{TE} \sin\left[\left(\Delta\varphi_t\right)_{TE} - \left(\Delta\varphi_t\right)_{LE}\right] \frac{\sin(\beta + \gamma)}{\cos(\gamma + \theta/2)} \tag{19}$$

was used. (This equation also involves iteration.) It was derived from Fig. 2 upon assuming planar geometry and neglecting the difference between C and C' (Kurkov, 1988). The angles $\Delta\varphi_t$ are measured averaged quantities.

One can now estimate the direction of $\hat{\mathbf{C}}_a$ by rotating $\mathbf{C}$ in the plane perpendicular to $\hat{\mathbf{n}}_{c\ell}$ by the angle $\theta/2$. The magnitude of $\mathbf{d}_t$ is again computed by using the fact that its end points subtend the measured $\Delta\varphi_t$'s and lie on a constant R. This allows one to compute $\mathbf{h}_t$ as described previously and to estimate coordinates of points A' as follows:

$$\mathbf{r}_{A'} \cong \mathbf{r}_A + \mathbf{h}_t$$

Once these coordinates are obtained, vector $\mathbf{C}_a$ can be recalculated and the new iteration can be started. The resulting $\mathbf{C}'$ at the end of iteration is used to obtain the absolute twist angles as described previously.

RESULTS

Experimental Variables

The complete results are given for three blades designated as F11, F1, and F7, which are all forward rotors of the twin-rotor counterrotating unducted fan model. The rotor speed was varied from a low reference speed to the design value. However, for the F11 blade the rotor speed achieved in the test was only 0.952 of the design. Table I lists the initial conditions for this test. The Z coordinate was normalized by using its maximum value at the leading edge.

Detailed results for the displacements of the leading and trailing edges normal to the average chord direction, and the absolute twist angles, are presented first in tabular form for the design (or maximum) speeds. Deflections are then presented graphically to illustrate their variation with speed as well as the agreement between experimental and predicted values.

In addition to experimental deflections the tables include calculated deflections incorporating the laser beam slip effect and the rigorous deflections obtained by strictly following leading- and trailing-edge blade particles. By comparing these two deflections the error associated with laser beam slip can be evaluated. The tables for twist angles also include predicted results calculated by using the constant-chord-length assumption; hence, the effect of this assumption can also be evaluated. (This assumption is used when calculating twist from experimental data.)

The deflections in the tables are signed quantities where the positive sign is as defined in Fig. 2. (Eqs. (12) and (17) yield correct signs.) Note, however, that when constructing vectorial deflections, one should take the absolute value of the tabulated quantities as the true magnitude associated with the appropriate unit vector.

Leading- and Trailing-Edge Displacements

Leading- and trailing-edge displacements perpendicular to the chord (i.e., bending displacements) are given in Table II. The table includes signed deflections and the associated normal unit vectors that define the appropriate planes. Superscripted h and $\hat{\mathbf{n}}$ symbols in the column headings allow the differentiation between three types of tabulated results. A bar above a symbol indicates the no-slip condition, a tilde indicates experimental results, and unmodified h and $\hat{\mathbf{n}}$ indicate predicted results with the slip effect.

Deflections h_t in Table II were not calculated for the no-slip condition because the definition of h_t requires some slip along the blade relative to the original undeflected reference point. On the other hand, for the experimental results $\tilde{h}$ was not available because the measurement is performed with only one laser beam, and $\tilde{h}_t$ must serve as an approximation to $\tilde{h}$.

Examining first the two groups of columns in Table II, one finds that h and the associated unit vector $\hat{\mathbf{n}}_{ch}$ are good approximations to $\tilde{h}$ and $\hat{\tilde{\mathbf{n}}}_{ch}$. Slight improvement is achieved by projecting h onto a

plane perpendicular to $\hat{n}_h$ (i.e., h_p). However, predicted results with slip show that up to about 7.5-percent error (for the F1 blade) can result by approximating h_p with h_{tp} (or h with h_t). As already mentioned, this error arises because the displacement along the laser beam cannot be measured. Figure 7 illustrates variation of $\tilde{h}_{tp}$ with speed and includes predicted $\bar{h}_p$ at the design condition as well as corrected experimental $\tilde{h}_{tp}$. The abscissa in Fig. 7 $\left(N_f^2\right)$ is the square of the ratio of rotational speed to the design rotational speed. The correction is derived from simulated experimental results. The measured displacements in the third group of columns in Table II were not corrected. The measured bending deflections in Fig. 7 are all higher than predicted, but, in general, the agreement is reasonable.

Twist Angles

Table III presents results for absolute twist angles. Note that positive twist corresponds to a β angle increase relative to the reference value. In addition to the apparent total twist angle (plane $\hat{n}_c$), twist angles in the initial plane $\hat{n}_{c\ell}$, in the average bending plane $\hat{n}_h$, and perpendicular to the pitch axis $\hat{k}$ are also given in the table. The first three groups of columns from the left are associated with the same results as for bending (i.e., with the true predicted twist angle, the predicted twist angle that includes the laser beam slip effect, and the measured absolute twist). The fourth group of columns was added in these tables to evaluate the effect of the constant-chord-length assumption made in calculating twist angles from measurements. The θ_n'' and $\hat{n}''$ are derived identically as in the experiment except that the measured angles in the tangential direction $\Delta\varphi_t$ are obtained from predicted blade contours. Thus subtracting θ_n from θ_n'' gives the correction factor associated with the constant-chord-length assumption. Comparing the appropriate unit vectors from column groups two and four indicates how this assumption affects the orientation of the associated planes.

Comparing group one and two results ($\bar{\theta}$ and θ) in Table III shows the error associated with the slip effect to be appreciable. Thus vectorial subtraction of the associated twist angles gives absolute errors of 0.53°, 0.41°, and 0.65° for the F11, F1, and F7 blades, respectively. However, the maximum errors for these blades for the planes defined by $\hat{n}_{c\ell}$, $\hat{n}_h$, and $\hat{k}$ unit vectors are respectively 0.10°, 0.12°, and 0.16°. On the other hand, comparing θ and θ'' indicates that the error associated with the constant-chord-length assumption is fairly independent of $\hat{n}$. The error is the largest for the F7 blade, amounting to about 0.2°. Considering now both the slip and the constant-chord-length errors, the maximum error is less than about 1/8° for any of the planes defined by $\hat{n}_{c\ell}$, $\hat{n}_h$, or $\hat{k}$ unit vectors. It is simplest therefore to choose the XY plane defined by the $\hat{k}$ unit vector for reporting the twist angles. The experimental measurement error associated with this test is estimated to be less than 1/4°.

If desired, the measured twist angles can be corrected for these two systematic errors. The correction is more accurate the closer the predicted and experimental twist angles are. However, even a rough estimate can considerably reduce these errors. For example, for a 50-percent error in estimating this correction, in the present case the total systematic measurement error would be reduced to 1/16°. In the plots presented in Fig. 8 the measured twist angles include corrected points (square symbols) at the design speed so that the effect of correction can be evaluated. Also included in Fig. 8 are the true predicted absolute twist angles $\bar{\theta}_k$ at the design speed. In general, the agreement between predicted and experimental twist angles, taking into account all blades in Fig. 8, is not very good.

Note that in Figs. 7 and 8 the first two points beyond the reference point (which is close to the origin of the axes) correspond to windmill conditions. Hence deflections for these points are attributed to centrifugal forces.

The results for the F21 blade, presented in Fig. 9, are significant because the deflections for this blade are the largest and the agreement between predicted and measured deflections is the best. For this blade the complete finite-element outputs were unavailable, but rather only the blade sections (deflected and undeflected) associated with the plane defined by the unit vector $\hat{n}_{c\ell}$. Thus the true deflections ($\bar{\theta}$ and $\bar{h}$) and the slip-effect corrections could not be evaluated. (Which is why the results for this blade were not included in the tables.) Predicted results in Fig. 9 are therefore θ_k and h_p, and corrected twist includes only the chord correction effect. However, on the basis of previous results the good agreement between predicted and measured deflections demonstrated in Fig. 9 would likely prevail for true predicted deflections. The test conditions for the F21 blade were close to the nominal design conditions: N = 8085 rpm, Mach 0.8, and β = 61.8°. The leading- and trailing-edge Z coordinates corresponding to laser beam tangency points were 29.50 and 29.68 cm.

CONCLUDING REMARKS

The unducted fan blade deflections caused by centrifugal and aerodynamic loads were measured with a nonintrusive optical method that uses low-power, helium-neon lasers. The method was applied to four recently designed blade prototypes. Measurements were made in a plane nearly perpendicular to the pitch axis. Twist angles and leading- and trailing-edge bending deflections were obtained for the near tip span with the total systematic (and therefore correctable) error of less than 1/8°. The experimental measurement error was estimated to be about 1/4°.

The agreement between predicted and experimental bending deflections was generally fair. However, the agreement between the corresponding twist angles was poor, except for one blade prototype, for which it was very good.

REFERENCES

Nieberding, W.C., and Pollack, J.L., 1977, "Optical Detection of Blade Flutter in YF-100 Turbofan Engine," ASME Paper 77-GT-66. (NASA TM X-73573.)

Kurkov, A.P., 1984, "Measurement of Self-Excited Rotor-Blade Vibrations Using Optical Displacements," Journal of Engineering for Gas Turbines and Power, Vol. 106, No. 1, pp. 44-49.

Lawrence, C., and Meyn, E.H., 1985, "The Use of an Optical Data Acquisition System for Bladed Disk Vibration Analysis," Vibrations of Blades and Bladed Disk Assemblies, R.E. Kielb and N.F. Rieger, eds., ASME, New York, pp. 65-73.

Srinivasan, A.V., and Fulton, G.B., 1984, "Advanced Turboprop Vibratory Characteristics," R84-956627-1, United Technologies Research Center, East Hartford, CT, NASA CR-174708.

Taylor, L.M., 1935, "Sighting Devices for Propeller Blade Observations," Air Corps Technical Report 4160, Dec. 7.

Stargardter, H., 1977, "Optical Determination of Rotating Fan Blade Deflections," Journal of Engineering for Power, Vol. 99, No. 2, pp. 204-209.

Sullivan, J.T., 1987, "Aerodynamic Performance of a Scale-Model, Counter-Rotating Unducted Fan," Advanced Technology for Aero Gas Turbine Components, AGARD CP-421, AGARD, Paris, pp. 22-1 to 22-16.

Kurkov, A.P., 1988, "Optical Measurement of Propeller Blade Deflections," NASA TP-2841, 1988.

TABLE I. - TEST VARIABLES

Blade	Design rotational speed, rpm	Test speed fraction	Nominal blade angle, β_{nom}	Mach number	Z/Z_{max} fraction	
					Leading edge	Trailing edge
F11	8089	0.952	60.3	0.80	0.973	0.960
F1	8185	.996	57.1	.72	.975	.973
F7	8314	.993	58.5	.72	.963	.961

TABLE II. - BENDING DEFLECTIONS

Blade	Symbol	Plane	True predicted				Predicted with slip				Experimental (relative to reference point)			
			$\bar{h}$, cm	$\hat{n}$			h, cm	$\hat{n}$			$\tilde{h}$, cm	$\hat{n}$		
				$\hat{i}$	$\hat{j}$	$\hat{k}$		$\hat{i}$	$\hat{j}$	$\hat{k}$		$\hat{i}$	$\hat{j}$	$\hat{k}$
F11	h	$\hat{n}_{ch}$	0.6375	-0.0601	-0.0801	0.9950	0.6347	-0.0970	-0.0550	0.9938	------	-------	-------	------
			.8334	-.1051	-.0423	.9936	.8245	-.1704	.0073	.9853	------	-------	-------	------
	h_p	$\hat{n}_h$	.6345	-.1342	-.0176	.9908	.6340	-.1338	-.0239	.9907	------	-------	-------	------
			.8329	-.1342	-.0176	.9908	.8235	-.1338	-.0239	.9907	------	-------	-------	------
	h_t	$\hat{n}_{t\ell}$	------	-------	-------	------	.6543	-.0844	-.0345	.9958	0.7419	-0.0837	-0.0349	0.9959
			------	-------	-------	------	.8486	-.1762	-.0019	.9843	.8903	-.1748	-.0026	.9846
	h_{tp}	$\hat{n}_h$	------	-------	-------	------	.6535	-.1338	-.0239	.9907	.7412	-.1339	-.0244	.9907
			------	-------	-------	------	.8479	-.1338	-.0239	.9907	.8893	-.1339	-.0244	.9907
F1	h	$\hat{n}_{ch}$	0.5311	-0.0448	0.0133	0.9989	0.5314	-0.0545	0.0183	0.9983	------	-------	-------	------
			.7506	-.0920	.0621	.9938	.7470	-.1291	.0953	.9870	------	-------	-------	------
	h_p	$\hat{n}_h$	.5298	-.0927	.0627	.9937	.5306	-.0926	.0575	.9940	------	-------	-------	------
			.7506	-.0927	.0627	.9937	.7460	-.0926	.0575	.9940	------	-------	-------	------
	h_t	$\hat{n}_{t\ell}$	------	-------	-------	------	.5710	-.0376	.0457	.9982	0.7196	-0.0359	0.0448	0.9983
			------	-------	-------	------	.7851	-.1405	.0796	.9869	1.0414	-.1393	.0789	.9871
	h_{tp}	$\hat{n}_h$	------	-------	-------	------	.5702	-.0926	.0575	.9940	.7186	-.0936	.0560	.9940
			------	-------	-------	------	.7841	-.0926	.0575	.9940	1.0404	-.0936	.0560	.9940
F7	h	$\hat{n}_{ch}$	0.8816	-0.0255	-0.0058	0.9997	0.8806	-0.0522	0.0100	0.9986	------	-------	-------	------
			.9698	-.0629	.0268	.9977	.9642	-.1238	.0723	.9897	------	-------	-------	------
	h_p	$\hat{n}_h$	.8786	-.0879	.0485	.9950	.8796	-.0877	.0408	.9953	------	-------	-------	------
			.9693	-.0879	.0485	.9950	.9629	-.0877	.0408	.9953	------	-------	-------	------
	h_t	$\hat{n}_{t\ell}$	------	-------	-------	------	.9144	-.0382	.0329	.9987	1.1984	-0.0372	0.0324	0.9988
			------	-------	-------	------	1.0124	-.1286	.0635	.9896	1.4879	-.1279	.0631	.9898
	h_{tp}	$\hat{n}_h$	------	-------	-------	------	.9134	-.0877	.0408	.9953	1.1971	-.0906	.0386	.9951
			------	-------	-------	------	1.0114	-.0877	.0408	.9953	1.4864	-.0906	.0386	.9951

TABLE III. - ABSOLUTE TWIST ANGLES

Blade	Twist angle	True predicted				Predicted with slip				Experimental (relative to reference point)				Predicted with slip and constant chord			
		$\bar{\theta}$, deg	$\bar{n}$			θ, deg	n			$\tilde{\theta}$, deg	$\hat{n}$			θ'', deg	$\hat{n}''$		
			$\hat{i}$	$\hat{j}$	$\hat{k}$		$\hat{i}$	$\hat{j}$	$\hat{k}$		$\hat{i}$	$\hat{j}$	$\hat{k}$		$\hat{i}$	$\hat{j}$	$\hat{k}$
F11	θ_{n_c}	2.6149	-0.2457	0.0788	0.9661	2.6305	-0.3904	0.2027	0.8980	2.1629	-0.4619	0.2661	0.8461	2.6869	-0.3786	0.1923	0.9054
	$\theta_{n_{c\ell}}$	2.5955	-.1533	.0023	.9882	2.4732	-.1533	.0023	.9882	1.9623	-.1533	.0023	.9882	2.5612	-.1533	.0023	.9882
	θ_{n_h}	2.5857	-.1342	-.0176	.9908	2.4652	-.1338	-.0239	.9907	1.9327	-.1339	-.0244	.9907	2.5331	-.1330	-.0243	.9908
	θ_k	2.5519	0	0	1.0000	2.3884	0	0	1.0000	1.8502	0	0	1.0000	2.4594	0	0	1.0000
F1	θ_{n_c}	2.8421	-0.2026	0.1766	0.9632	2.8783	-0.2986	0.2718	0.9148	4.2322	-0.2655	0.2390	0.9340	2.8447	-0.2904	0.2637	0.9198
	$\theta_{n_{c\ell}}$	2.8186	-.1129	.0883	.9897	2.7723	-.1129	.0883	.9897	4.1286	-.1129	.0883	.9897	2.7493	-.1129	.0883	.9897
	θ_{n_h}	2.8052	-.0927	.0627	.9937	2.7421	-.0926	.0575	.9940	4.0930	-.0936	.0560	.9940	2.7197	-.0915	.0569	.9942
	θ_k	2.7390	0	0	1.0000	2.6351	0	0	1.0000	3.9565	0	0	1.0000	2.6185	0	0	1.0000
F7	θ_{n_c}	1.3597	-0.3882	0.3127	0.8669	1.6552	-0.6060	0.5028	0.6164	4.3063	-0.3623	0.2903	0.8857	1.7790	-0.5558	0.4585	0.6935
	$\theta_{n_{c\ell}}$	1.2522	-.1019	.0669	.9925	1.1706	-.1019	.0669	.9925	4.0292	-.1019	.0669	.9925	1.3799	-.1019	.0669	.9925
	θ_{n_h}	1.2398	-.0879	.0485	.9949	1.1374	-.0877	.0408	.9953	3.9855	-.0906	.0386	.9951	1.3461	-.0862	.0402	.9955
	θ_k	1.1792	0	0	1.0000	1.0210	0	0	1.0000	3.8186	0	0	1.0000	1.2346	0	0	1.0000

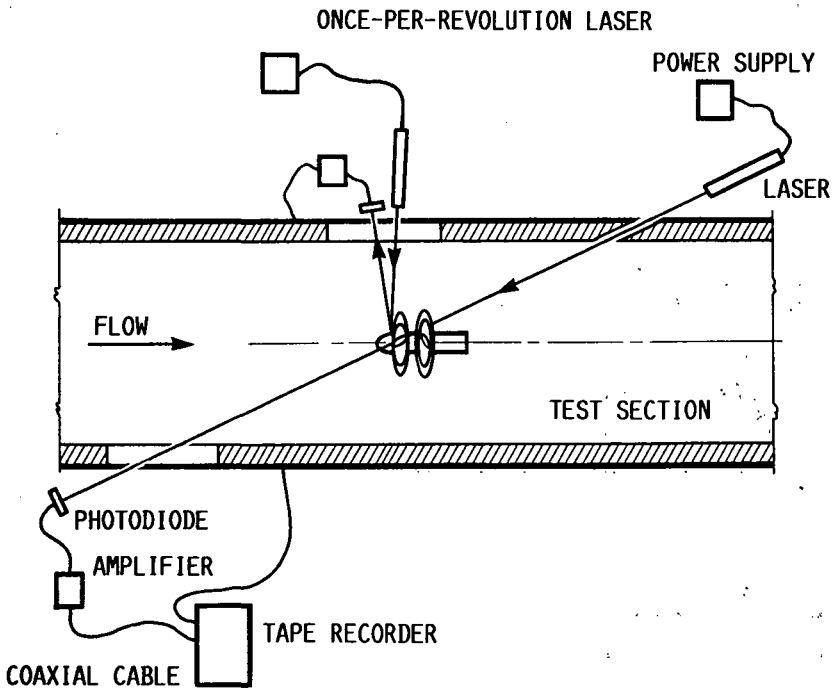

FIGURE 1. - TEST SCHEMATIC.

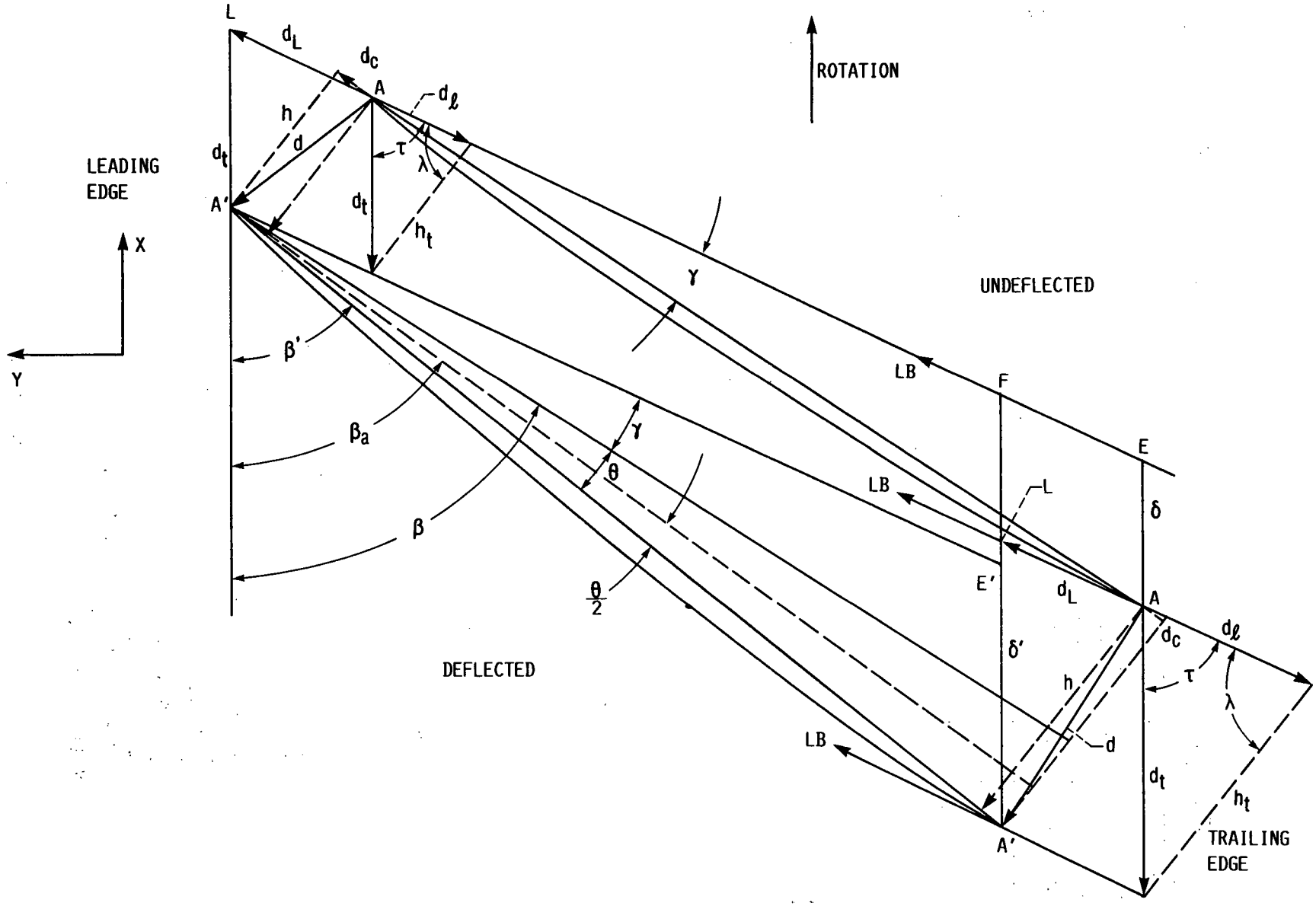

FIGURE 2. - GEOMETRY OF LASER BEAM AND BLADE SECTION.

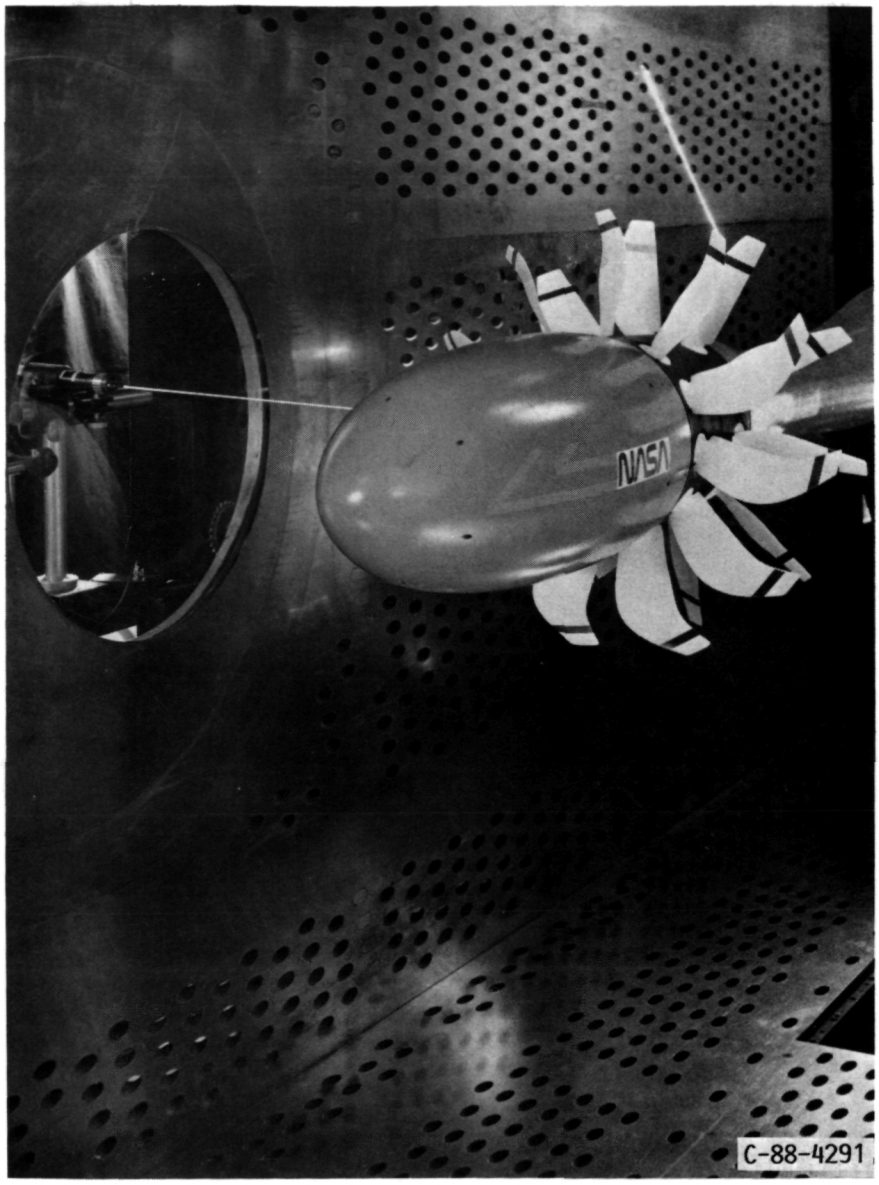

FIGURE 3. - COUNTERROTATING UNDUCTED FAN AND TWO LASERS INSTALLED IN THE 8- BY 6-FT WIND TUNNEL.

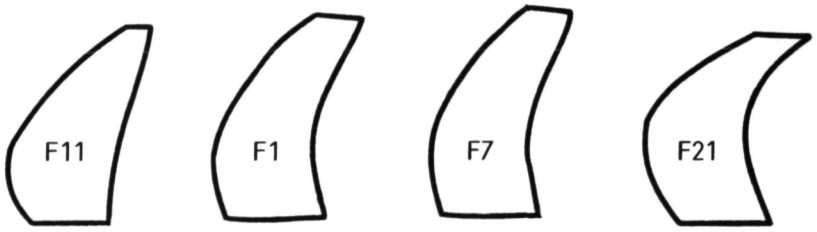

FIGURE 4. - BLADE SCHEMATICS, PLAN VIEW.

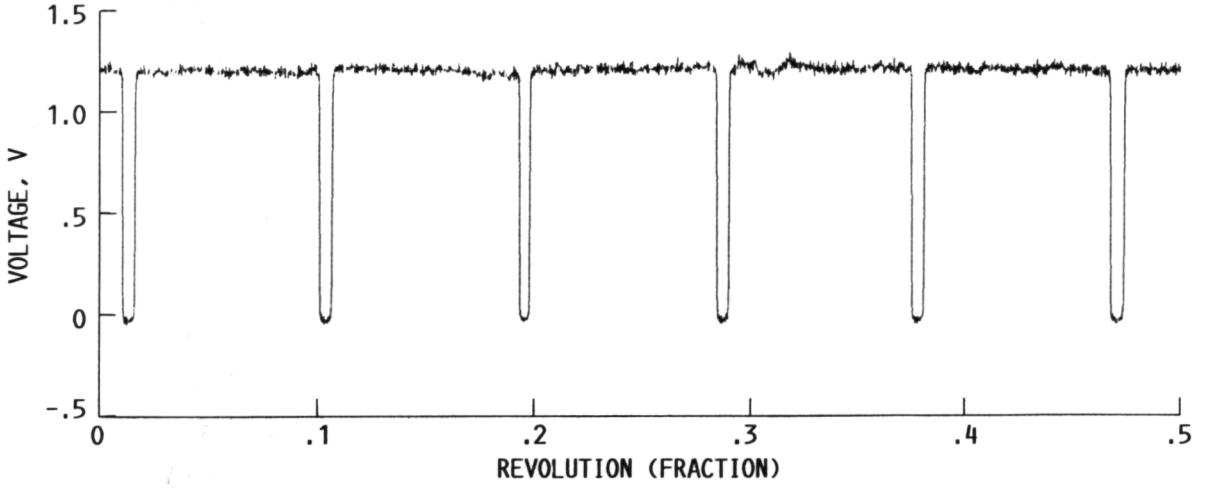

FIGURE 5. - BLADE-TIP PULSES, F11 BLADE.

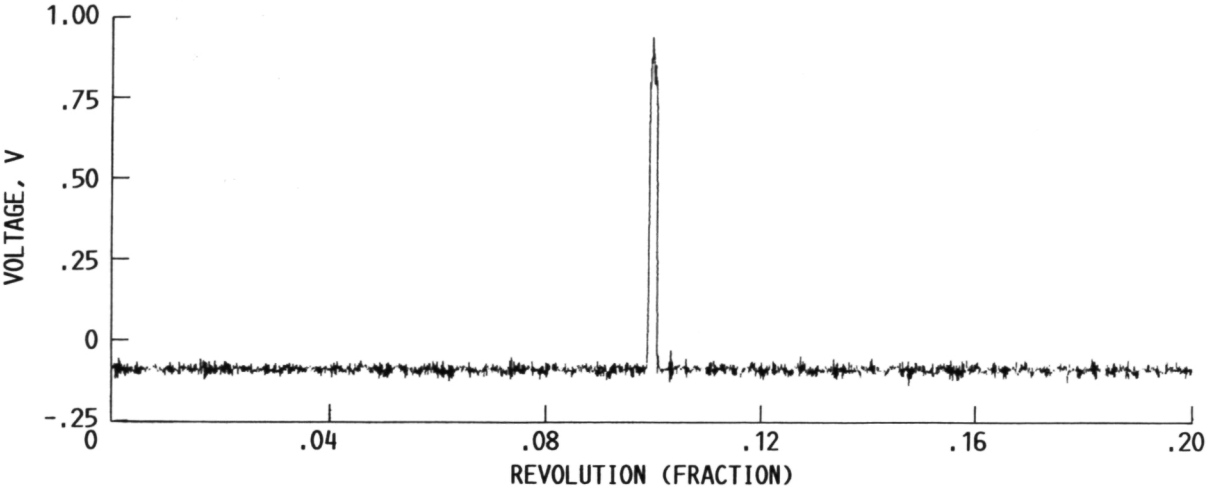

FIGURE 6. - ONCE-PER-REVOLUTION PULSE, F11 HUB.

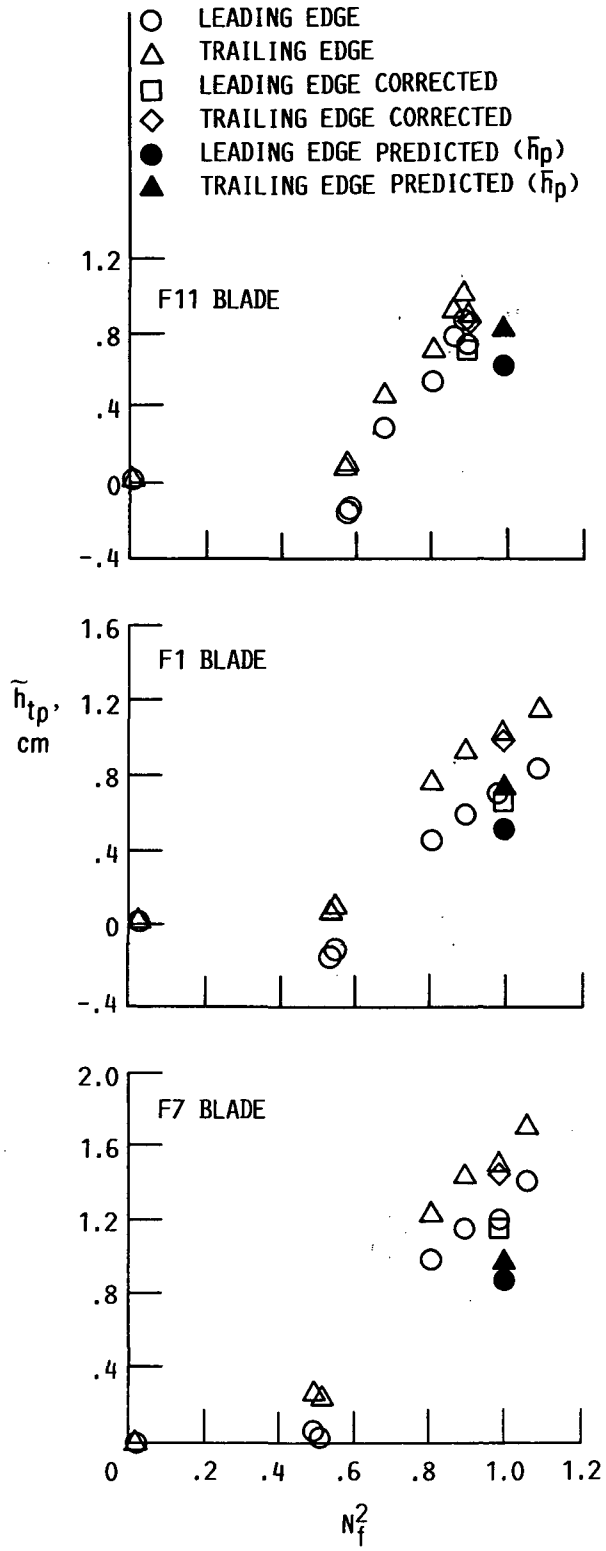

FIGURE 7. - BENDING DEFLECTIONS.

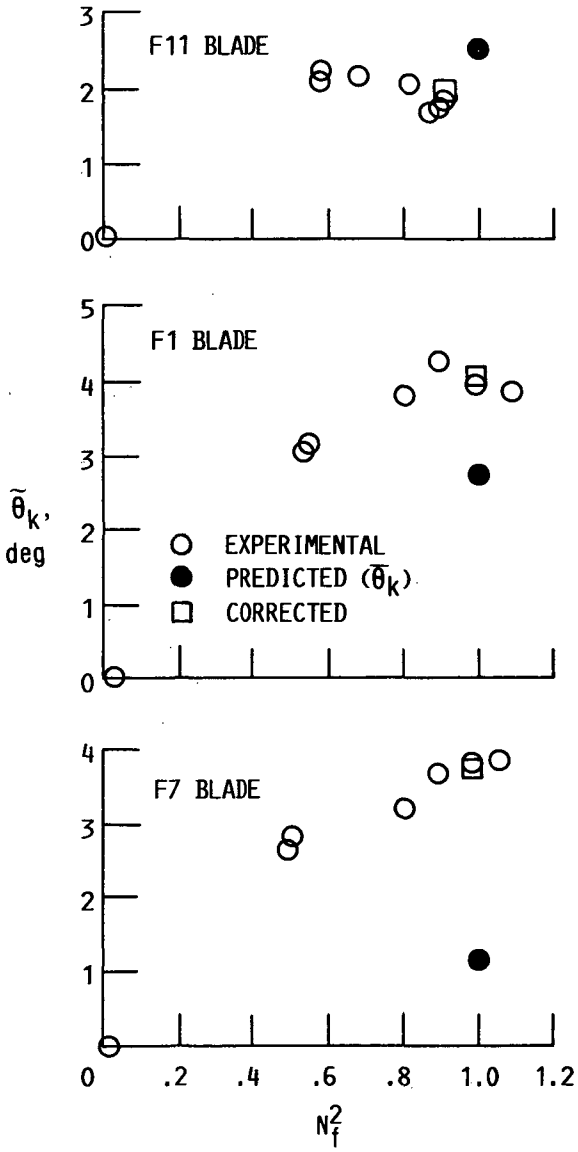

FIGURE 8. - ABSOLUTE TWIST ANGLE.

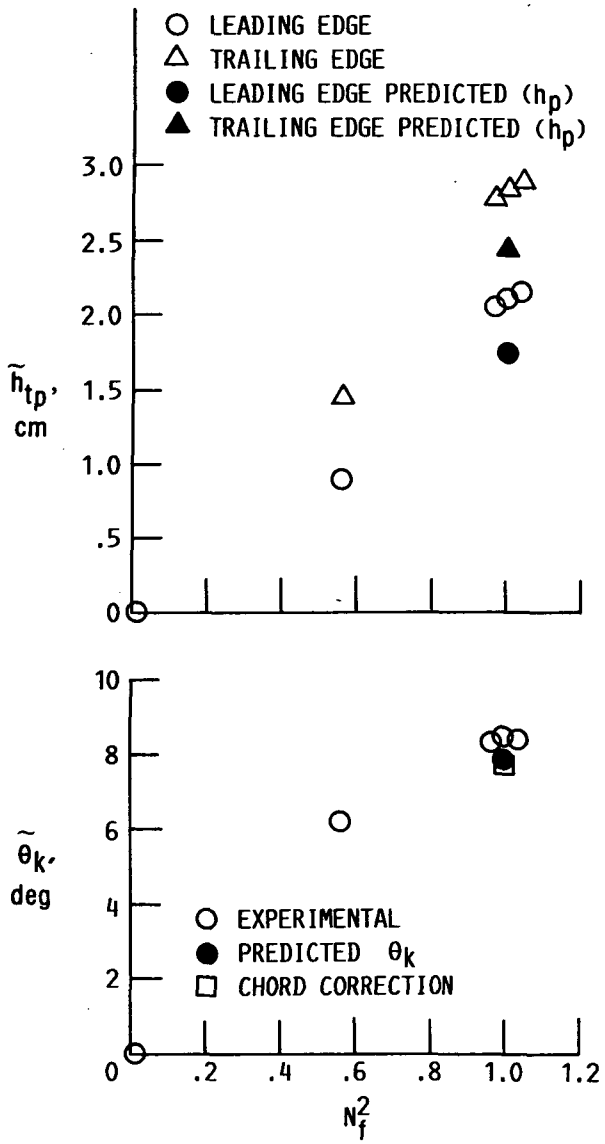

FIGURE 9. - BENDING AND TWIST DEFLECTIONS, F21 BLADE.

NASA
National Aeronautics and Space Administration

Report Documentation Page

1. Report No.	2. Government Accession No.	3. Recipient's Catalog No.
NASA TM-100966		

4. Title and Subtitle

Optical Measurement of Unducted Fan Blade Deflections

5. Report Date

6. Performing Organization Code

7. Author(s)

Anatole P. Kurkov

8. Performing Organization Report No.

E-4131-1

10. Work Unit No.

535-03-01

9. Performing Organization Name and Address

National Aeronautics and Space Administration
Lewis Research Center
Cleveland, Ohio 44135-3191

11. Contract or Grant No.

13. Type of Report and Period Covered

Technical Memorandum

12. Sponsoring Agency Name and Address

National Aeronautics and Space Administration
Washington, D.C. 20546-0001

14. Sponsoring Agency Code

15. Supplementary Notes

Prepared for the 34th International Gas Turbine and Aeroengine Congress and Exposition sponsored by the American Society of Mechanical Engineers, Toronto, Canada, June 4-8, 1989.

16. Abstract

A nonintrusive optical method for measuring unducted fan (or propeller) blade deflections is described and evaluated. The measurement does not depend on blade surface reflectivity. Deflection of a point at the leading edge and a point at the trailing edge in a plane nearly perpendicular to the pitch axis is obtained with a single light beam generated by a low-power, helium-neon laser. Quantitative analyses are performed from taped signals on a digital computer. Averaging techniques are employed to reduce random errors. Measured static deflections from a series of high-speed wind tunnel tests of a counterrotating unducted fan model are compared with available predicted deflections, which are also used to evaluate systematic errors.

17. Key Words (Suggested by Author(s))	18. Distribution Statement
Blade deflection Prop-fan Unducted fan Propeller	Unclassified - Unlimited Subject Category 35

19. Security Classif. (of this report)	20. Security Classif. (of this page)	21. No of pages	22. Price*
Unclassified	Unclassified	14	A02

*For sale by the National Technical Information Service, Springfield, Virginia 22161

National Aeronautics and
Space Administration

Lewis Research Center
Cleveland, Ohio 44135

FOURTH CLASS MAIL

ADDRESS CORRECTION REQUESTED

Official Business
Penalty for Private Use $300

Postage and Fees Paid
National Aeronautics and
Space Administration
NASA-451

NASA